UCID— 16792

Lawrence Livermore Laboratory

ONE-DIMENSIONAL CALCULATIONS: HIGH-EXPLOSIVE/NUCLEAR EFFECTIVENESS COMPARISONS IN WEAK TUFF

Charles M. Snell

Jon B. Bryan

April 1975

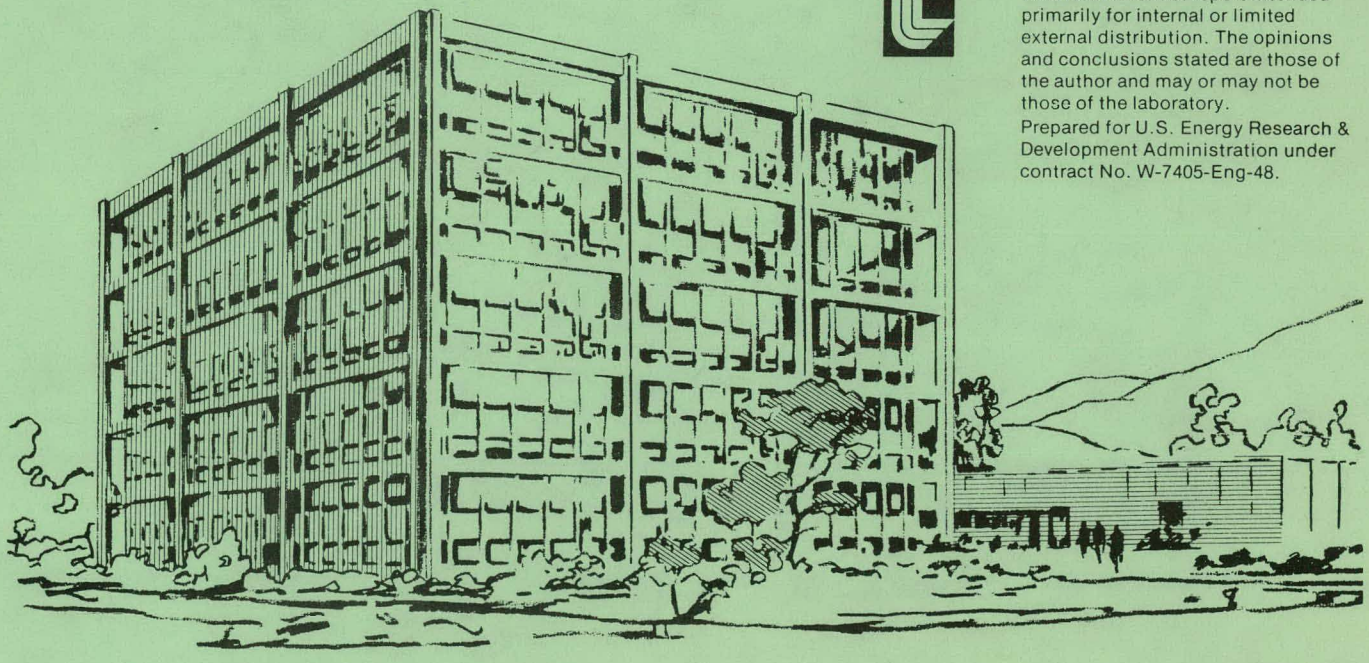

Prepared for U.S. Energy Research & Development Administration under contract No. W-7405-Eng-48.

DISCLAIMER

CONTENTS

ONE-DIMENSIONAL CALCULATIONS: HIGH-EXPLOSIVE/NUCLEAR EFFECTIVENESS COMPARISONS IN WEAK TUFF

ABSTRACT

One-dimensional Lagrangian computer calculations have been performed to model the effects of buried high-explosive and nuclear detonations in weak saturated tuff. Fundamental differences between shock propagation and energy coupling mechanisms for the nuclear and high-explosive detonations were noted.

The nuclear source was found to induce high peak stresses and particle velocities in the tuff environment, but long-term transfer of kinetic energy to the rock was more efficient for the high-explosive calculations. Total mound kinetic energy and long-lived material velocities are the most important factors that control crater formation from optimum-depth explosive detonations. Therefore, it is judged that the cratering effectiveness of a nuclear event will be correctly simulated by a high-explosive detonation of about 60% the nuclear energy yield. Integrated shock effects, degree of rock fracturing, and all interactions that occur over a time scale greater than a few milliseconds were properly matched with this similitude factor. However, peak velocities at the shock front were higher for the nuclear case; the transient shock peak and long-term dynamic effects cannot both be accurately modeled at the same time in this medium.

INTRODUCTION

Recently published studies were concerned with the relative cratering effectiveness of high-explosive and nuclear detonations in very weak saturated Bearpaw clay shale.[1,2] Both one-dimensional and two-dimensional Lagrangian finite-difference computer calculations were used to model shock transmission and cratering effects from buried explosive charges. Results indicated that the nuclear source was far less efficient in transferring kinetic energy to its environment than a high-explosive event of the same energy yield. Calculated dimensions of the nuclear crater were correspondingly smaller. At burial depths commonly used for cratering detonations, it was found that a high-explosive charge of one-half the nuclear energy yield accurately matched the late-time material velocities, overall mound kinetic energy, and final crater size of the nuclear calculation. The peak stresses and particle velocities near the shock front were somewhat higher for the nuclear source, particularly at close ranges; however, the long-term material velocities and overall mound energy proved far more important in simulating dynamic effects.

It was concluded that total kinetic energy transferred to the medium (one-dimensional calculations) or the somewhat more accurate mound kinetic energy (two-dimensional calculations) provide valid criteria for achieving similitude between high-explosive and nuclear cratering events. The transient peak of the shock front cannot be perfectly matched close to the source due to the intense high-frequency "spike" from the nuclear detonation. Nonetheless, a high-explosive source of one-half the nuclear energy yield provided excellent similitude of the overall material dynamics and cratering effects in Bearpaw clay shale.

SUITE OF CALCULATIONS

The similitude results summarized above apply only to low-strength saturated Bearpaw shale. The differing characteristics of other geologic media may significantly influence shock transmission and energy coupling efficiency. One material of interest is wet tuff, a porous weak rock found at certain potential high-explosive test sites. To establish approximate similitude requirements for this medium, a series of three calculations has been performed using the one-dimensional Lagrangian finite-difference computer code "SOC73," which incorporates continuum solid mechanics and failure models.[3] These calculations represent one-dimensional spherically symmetric shot configurations in a homogeneous free-field environment of almost infinite extent. No nearby free-surface is present to reflect the shock wave. No overburden pressure or depth dependence is included in the problems. Charge sizes and energy yields are chosen to be similar to typical high-explosive test events and to the previous calculations for Bearpaw shale. The three configurations will be denoted as follows:

NM10 A gelled nitromethane high-explosive source of 10 ton = 4.186×10^5 Mbar-cc energy yield (1 Mbar-cc = 10^5 joules or 10^{12} ergs), and an initial radius of 130.47 cm.

NM12 A gelled nitromethane high-explosive source of 12.26 ton = 5.132×10^5 Mbar-cc energy yield, and an initial radius of 139.64 cm.

NUC A hypothetical nuclear energy source region consisting of vaporized iron gas with an energy content of 20 tons (8.37×10^5 Mbar-cc). The source has an assumed initial density of 1.5 g/cc and a radius of 27 cm.

MATERIAL CONSTITUTIVE RELATIONS

Hydrodynamic calculations require a comprehensive material description or "equation of state" for each high-explosive, gaseous, or solid region in the problem. The model used to describe high-explosive energy release (detonation) and subsequent adiabatic expansion of the product gas is the Jones-Wilkins-Lee (JWL) equation of state.[4] The JWL parameters for gelled nitromethane were provided by the Organic Materials Division of the Lawrence Livermore Laboratory[5]; these are listed in Table 1. The model of

Table 1. Basic physical properties and Jones-Wilkins-Lee parameters for gelled nitromethane explosive.

Property	Value
Bulk density (g/cc)	1.21
Detonation velocity (m/sec)	6210
Chapman-Jouguet Mu	0.34614
Chapman-Jouguet pressure (Mbar)	0.120
Energy release (Mbar-cc/cc)	0.045
R_1	4.90
R_2	1.40
A	3.18
B	0.06378
Omega	0.38

Butkovich[6] is used to obtain pressure-volume-energy equations of state for the nuclear source region of iron gas, the wet rock vaporized by the nuclear source, and the water component within the rock vaporized to somewhat longer range.[6]

Finally, constitutive relations for the solid wet tuff material were developed from a simple-mixture compressibility model.[7] This technique simulates the pressure versus volumetric strain behavior (P-Mu compressibility curves*) of a rock-water-air matrix, using only the basic physical and elastic properties of the composite as input. The shear strength as a function of mean confining pressure (K-P_m curve) is also predicted. Basic physical properties assumed for the tuff material are summarized in Table 2; these properties are quite similar to the average characteristics of saturated Diamond Mine tuff, a Nevada Test Site rock in which earlier experiments have been conducted.

The P-Mu relationship generated using the listed properties is shown in Figs. 1a and 1b for high and low pressure ranges, respectively, with the Bearpaw shale curve also presented for comparison. Figure 2 shows the shear strength curve for saturated tuff as a function of mean pressure (K-P_m). The loading and unloading compressibility curves are virtually identical in this case because the material is almost (99.4%) fully saturated (very little hysteresis or permanent removal of air voids occurs upon compression); therefore, only a single P-Mu curve is shown in Fig. 1a. The loading and unloading (compacted) P-Mu curves in Fig. 1b reveal a small amount of hysteresis at very low pressures, corresponding to the small amount of air void porosity (≈0.22%)

---

* Volumetric strain $Mu = \frac{V_o}{V} - 1$

where V_o = initial specific volume of rock matrix at zero pressure
V = specific volume at pressure "P"

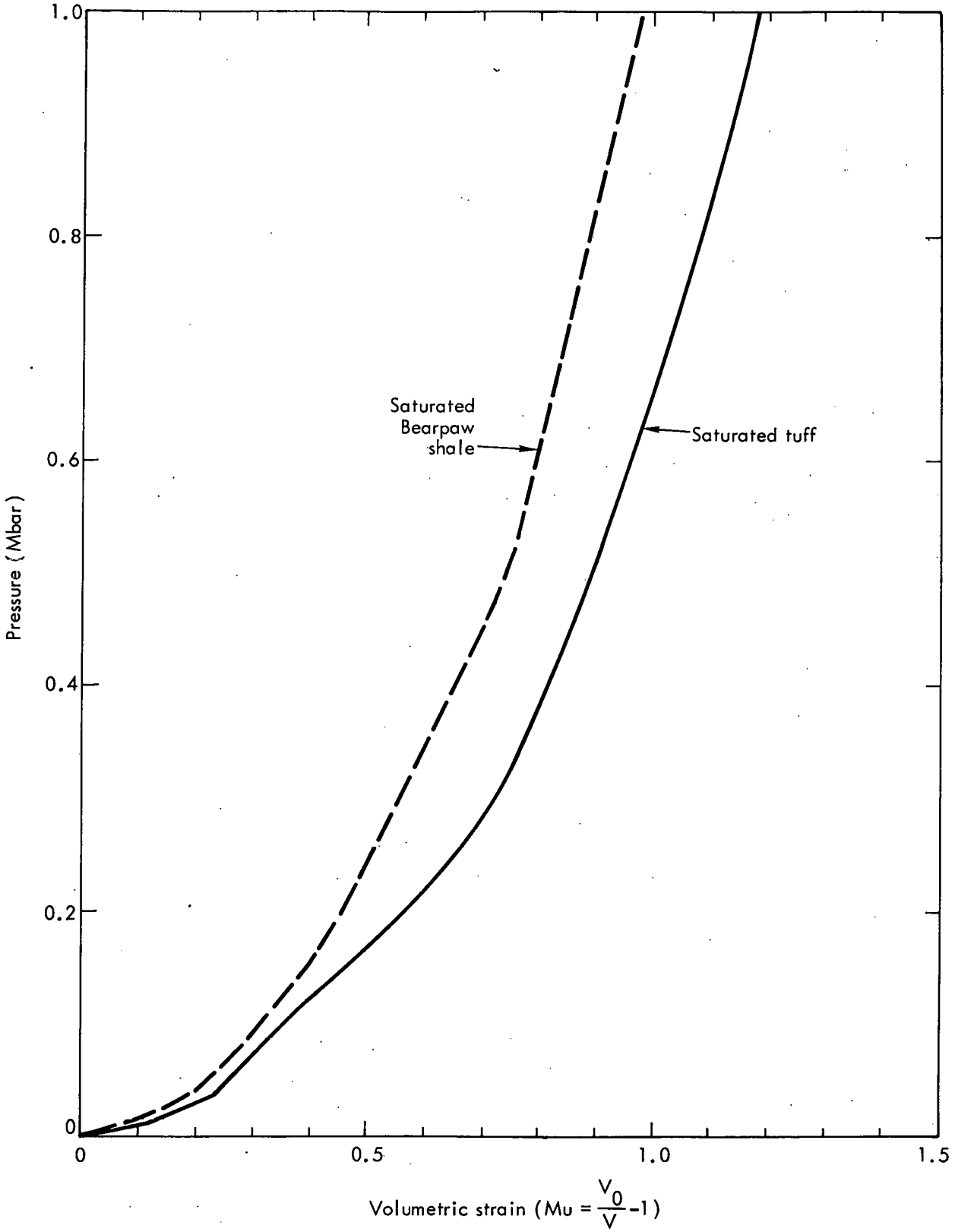

Fig. 1a. High-pressure P-Mu compressibility curves for Bearpaw shale and saturated tuff.

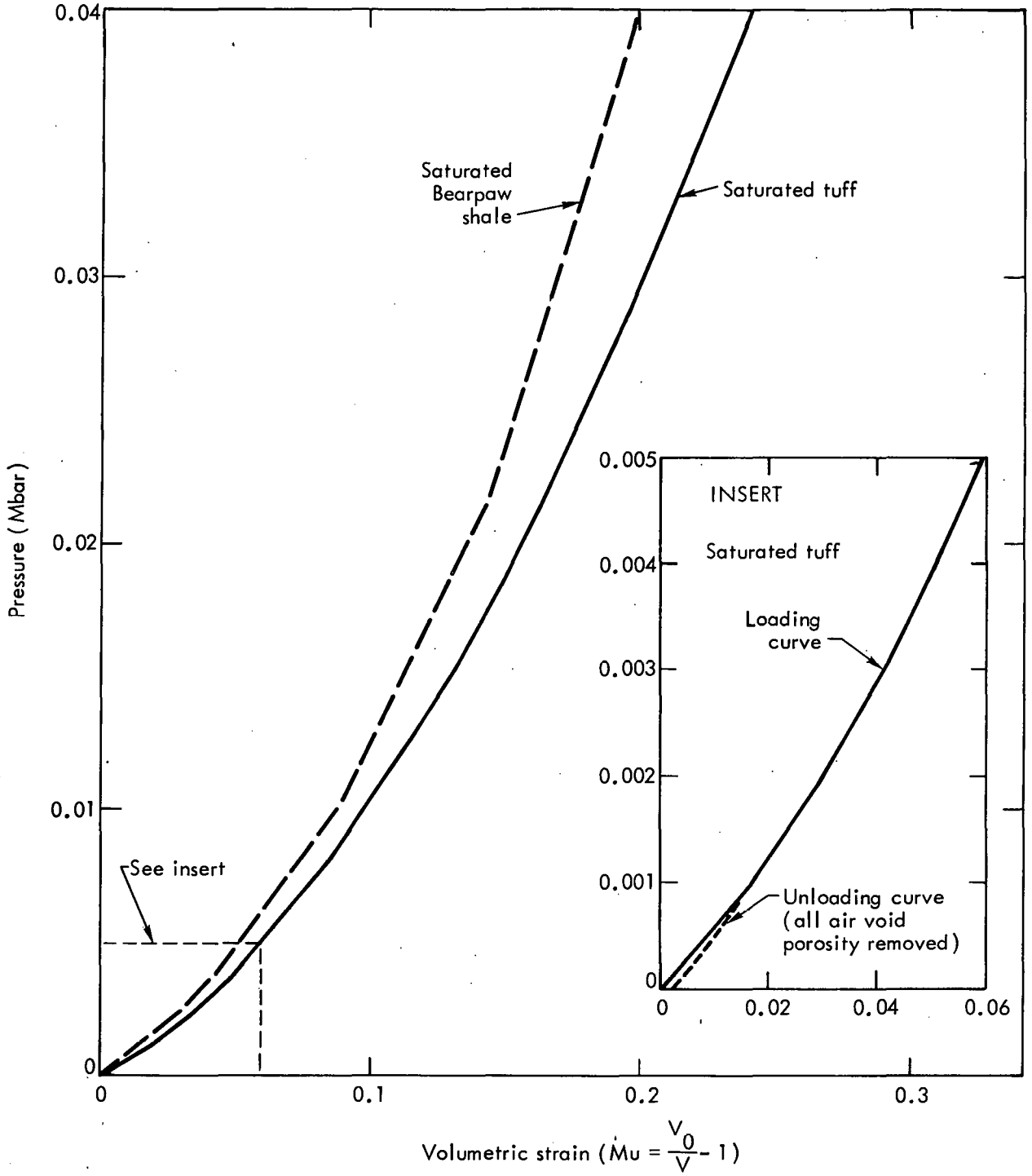

Fig. 1b. Low-pressure P-Mu compressibility curves for Bearpaw shale and saturated tuff.

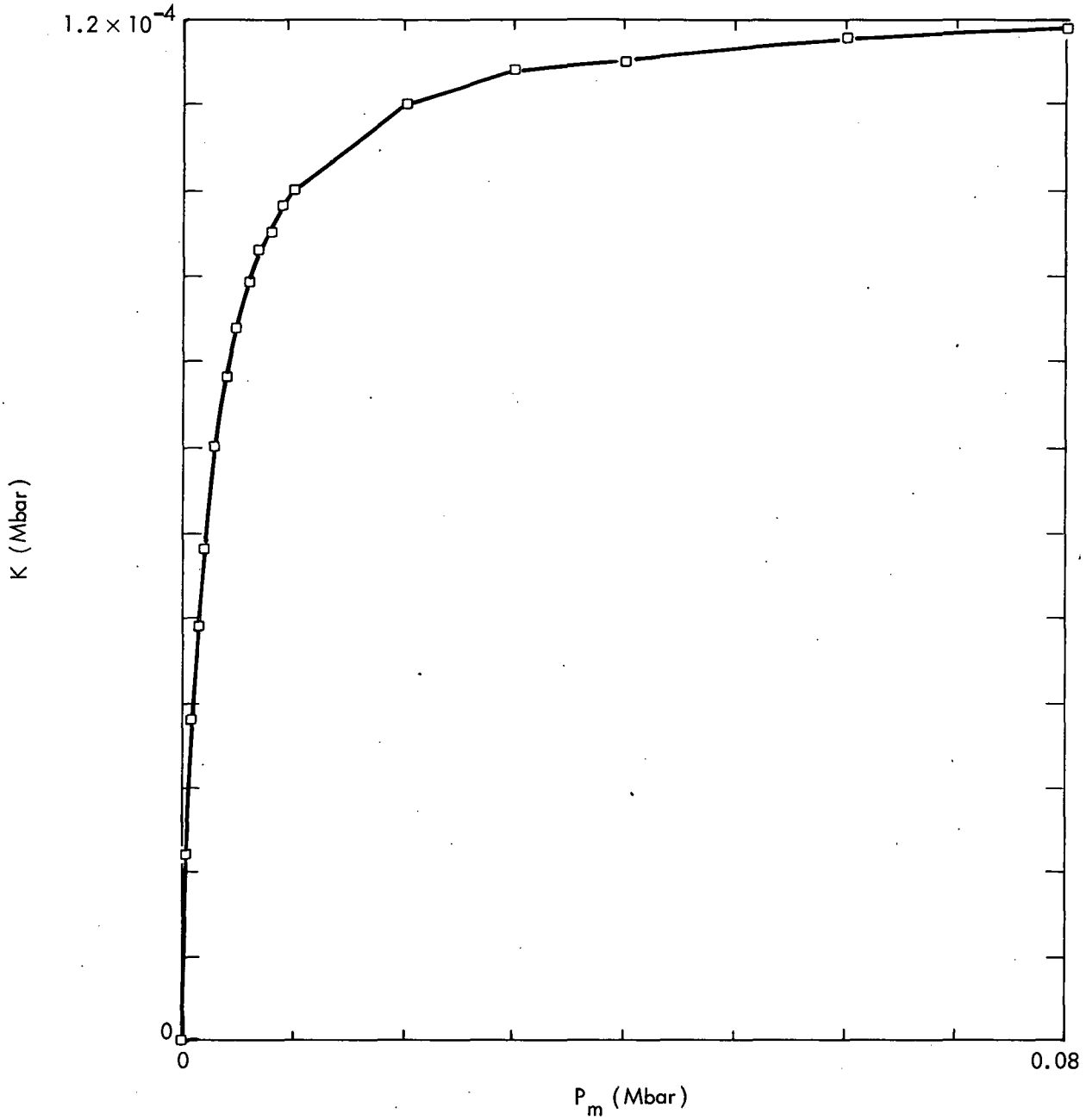

Fig. 2. K-P_m shear strength curve for saturated tuff (shear stress at failure initiation "K" as a function of mean confining pressure "P_m").

Table 2. Assumed physical properties of the saturated tuff (compared with average in situ values for the Diamond Mine tuff[8] material).

Property	Assumed value	In Situ value
Bulk density (g/cc)	1.92	(≈1.9)
Rock grain density (g/cc)	2.4058	
Total porosity (%)	34.4	
Air-filled porosity (%)	0.2225	
Saturation (%)	99.4	
Water content (fraction by weight)	0.178	
Initial bulk modulus (kbar)	70.4	(72)
Initial shear modulus (kbar)	36.3	(33.6)
Compressional sonic velocity (m/sec)	2488	(2480)
Poisson's ratio	0.28	(0.296)
Ultimate shear strength (kbar)	0.119	
Tensile strength (kbar)	0.0	

removed from the material. Note that the ultimate shear strength is a relatively low 119 bars (Fig. 2), as would be expected for a porous wet medium. The tuff is assumed to have no tensile strength at $P_m = 0$. The exact tensile strength and low-pressure strength behavior assumed have little influence upon the early-time free-field calculations discussed here. This type of rock falls between Bearpaw shale and the denser "competent" rocks in strength and most other physical properties. It is, however, similar to Bearpaw shale in possessing a high water content and low air void porosity.

SIMILITUDE REQUIREMENTS

To properly interpret results of the similitude comparison calculations, it is necessary to examine the basic differences between high-explosive and nuclear phenomenology. The inefficient energy coupling that occurs for buried nuclear events is attributed to the short time-scale of energy release (less than 10^{-3} msec) and to the correspondingly high peak pressures experienced at locations close to the device. These conditions cause vaporization of the adjacent rock, and cause material somewhat further from the detonation to be loaded onto the high-pressure section of the Hugoniot. Such high-pressure loading is extremely inefficient for converting shock energy to kinetic energy of the rock. The upper portion of the Hugoniot is very steep (material is quite stiff), thus little added "PdV" work is done by high-pressure loading and release. Most of the additional energy deposited by the passing shock wave is lost as internal waste heat, which does no useful work in moving the material.[1]

High-explosive detonations, on the other hand, release energy over a longer period of time (about 0.25 msec for this geometry) and over a relatively larger volume of space.

The peak pressures achieved are only about 100 kbar. Material vaporization effects are usually negligible, and loss of energy as waste heat is less severe. The large non-condensable explosive gas sphere also provides kinetic energy over a relatively longer time period, since the expanding bubble maintains high stress levels in the surrounding rock and continues to transfer significant energy by cavity expansion. This expansion is primarily responsible for driving material flow behind the shock front. For these reasons, long-term kinetic energy transfer to the environment is more efficient for a high-explosive event than for a nuclear event of the same yield.

It is important to recognize that the differences between nuclear and high-explosive events are related to the source characteristics and are therefore time-dependent. The small high-pressure nuclear source produces an intense shock wave which rapidly couples kinetic energy to the immediate environment. The early-time peak velocities and stresses close to the event are quite high. At later times, the efficient transfer of energy from the large high-explosive (HE) cavity becomes a predominant factor. Kinetic energy coupled from the slow-acting HE source overtakes and surpasses a nuclear event of the same yield. The time required for the coupling process depends on the size scale and energy release of the event, and on the material properties. The one-dimensional "infinite-medium" calculations in saturated Bearpaw shale demonstrated that coupling of energy from the cavity into kinetic energy of material was almost complete at times of about 3 to 10 msec for HE events (energy yield of 10 to 20 tons).

Energy coupling for cratering detonations is also influenced by reflection at the free surface. Two-dimensional calculations showed that the characteristic energy coupling time for typical buried cratering detonations was about twice the source-to-surface signal transmission time, or about 10 to 12 msec for 10- to 20-ton events. After this time, the direct and reflected waves had traveled beyond the immediate crater vicinity and the ejecta velocity field was well stabilized. Based on these results for Bearpaw shale, it was decided to carry the one-dimensional tuff calculations to a total time of 20 msec. Similitude between HE and nuclear events may then be established by comparing residual velocities or kinetic energies in rock at late times, after the velocity fields are stabilized.

The high-explosive/nuclear similitude factor is estimated by assuring that the total kinetic energies in rock (or the residual velocities behind the shock front) are closely comparable for the HE and nuclear events. This condition was fulfilled in the Bearpaw shale calculations with an HE yield of one-half the nuclear source energy. However, basic physical properties of the tuff medium differ significantly from those of Bearpaw shale. The initial density of tuff is about 13% lower, and the bulk modulus is significantly lower at the intermediate pressures achieved by HE detonations. The bulk modulus of the tuff begins to decrease slightly at 100 kbar (see Fig. 1a) due to the quartz solid-solid phase transition in this pressure range; pressures above 100 kbar are achieved only for the nuclear event. Poisson's ratio for tuff is 0.28, as compared with a nominal assumed value of 0.48 for Bearpaw shale.[9] Thus, shear moduli for the

tuff are always much higher and the material does not share the almost-fluid low shear stress behavior of the Bearpaw shale. Due to the increased shear moduli, the initial sonic velocity and shock propagation velocities at low pressures are significantly greater for the tuff than for Bearpaw shale. Finally, the average strength of the tuff is about a factor of ten higher, and this significant shear strength exerts a noticeable influence on wave propagation at stress levels of interest. These differences generally contribute toward efficient transmission of the high-frequency nuclear shock peak in the tuff, thereby decreasing the apparent gap between nuclear and HE effectiveness. One might therefore anticipate changes in the stress wave transmitted and a shift in the similitude requirements between Bearpaw shale and tuff. These expectations were borne out in part by the calculations. Nonetheless, other more subtle effects acted to nullify these trends, and the final similitude factor was not greatly modified from the value previously found for Bearpaw shale. Detailed results are discussed in the next section.

CALCULATIONAL RESULTS

Successful similitude analogs in the Bearpaw shale study were the 10-ton high-explosive (H10) and 20-ton nuclear (N20) configurations.[1,2] Hence, the first two tuff calculations, "NM10" and "NUC," used 10-ton high-explosive and 20-ton nuclear energy yields, respectively. A priori considerations discussed above led to the belief that HE and nuclear effectiveness values might differ by less than a factor of two for the tuff medium. Therefore, an additional high-explosive calculation closer to the nuclear standard energy was also undertaken. This calculation, denoted as "NM12," had an energy yield of 12.26 tons.

Shock peak arrival times as a function of range for the three calculations are shown in Fig. 3. The "NM12" peak slightly precedes "MN10" due to the greater radius of the HE source (high detonation velocity in the source). The nuclear peak dramatically leads both of the high-explosive arrivals because of the extremely high pressures and shock velocities close to the nuclear event. Note that the peak of the nuclear stress wave remains about 0.7 msec ahead of the high-explosive signals at longer ranges, where the transmission velocities have become nearly equal. Thus, nuclear effects will initiate somewhat sooner at a given range than the high-explosive effects. This fact must be kept in mind when examining results. The transmission velocity of the peak pulse approaches a value of about 1700 m/sec at ranges beyond 10 meters. This is somewhat slower than the sonic velocity of 2488 m/sec (straight line in Fig. 3) because the arrival times of the gradually diffusing peak (rather than the initial front arrivals) have been plotted. The peaks and post-peak behavior are of greatest interest with regard to the phenomena discussed here.

Calculated shock waveforms as a function of time at a range of 8 meters from the problem center are shown in Fig. 4a (radial stress pulse waveforms) and Fig. 4b (particle velocity waveforms). The nuclear shock wave arrives sooner and the peak values exceed the HE calculations by about a factor of two. However, a major deviation of the opposite

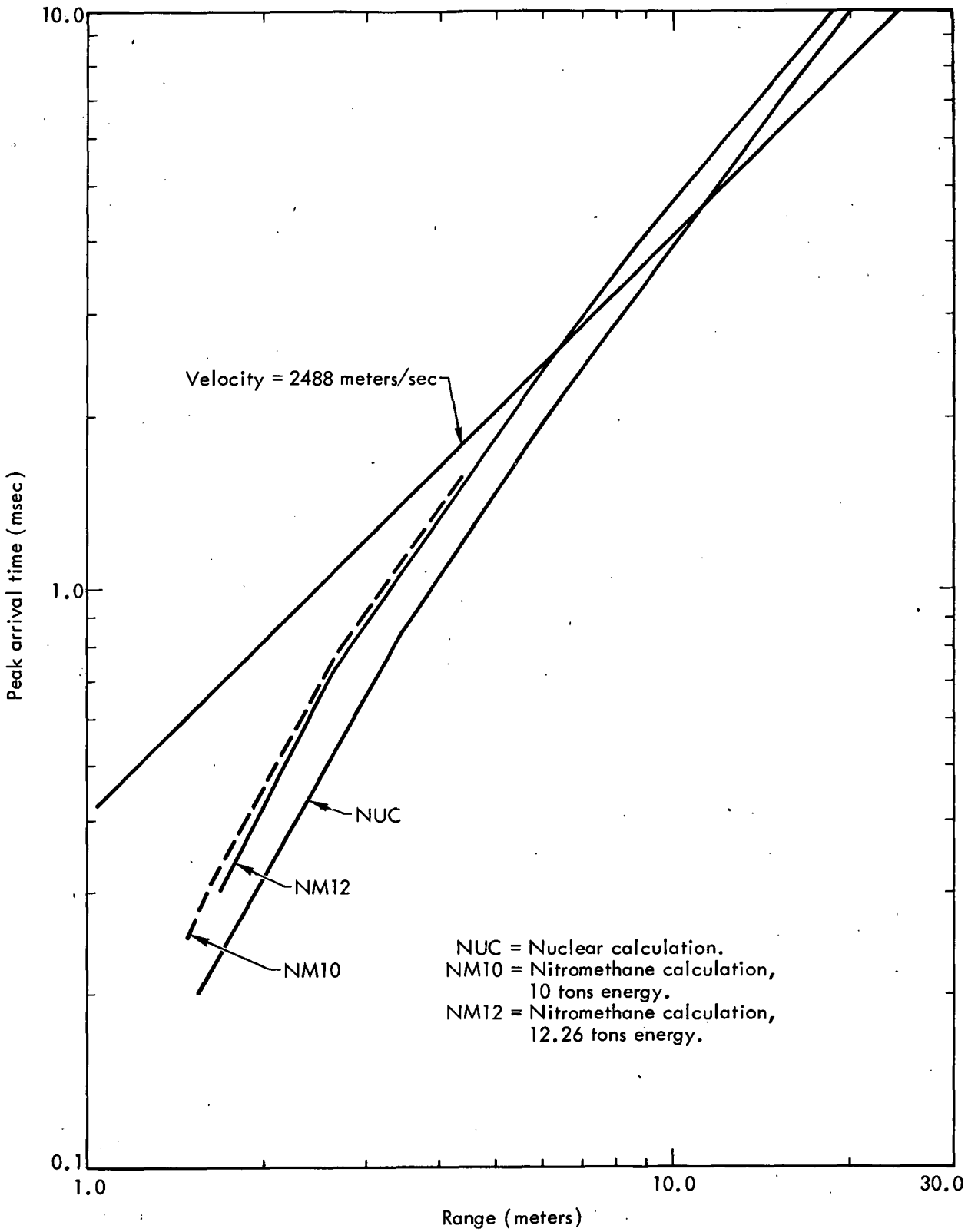

Fig. 3. Approximate shock front peak arrival time as a function of initial range "R."

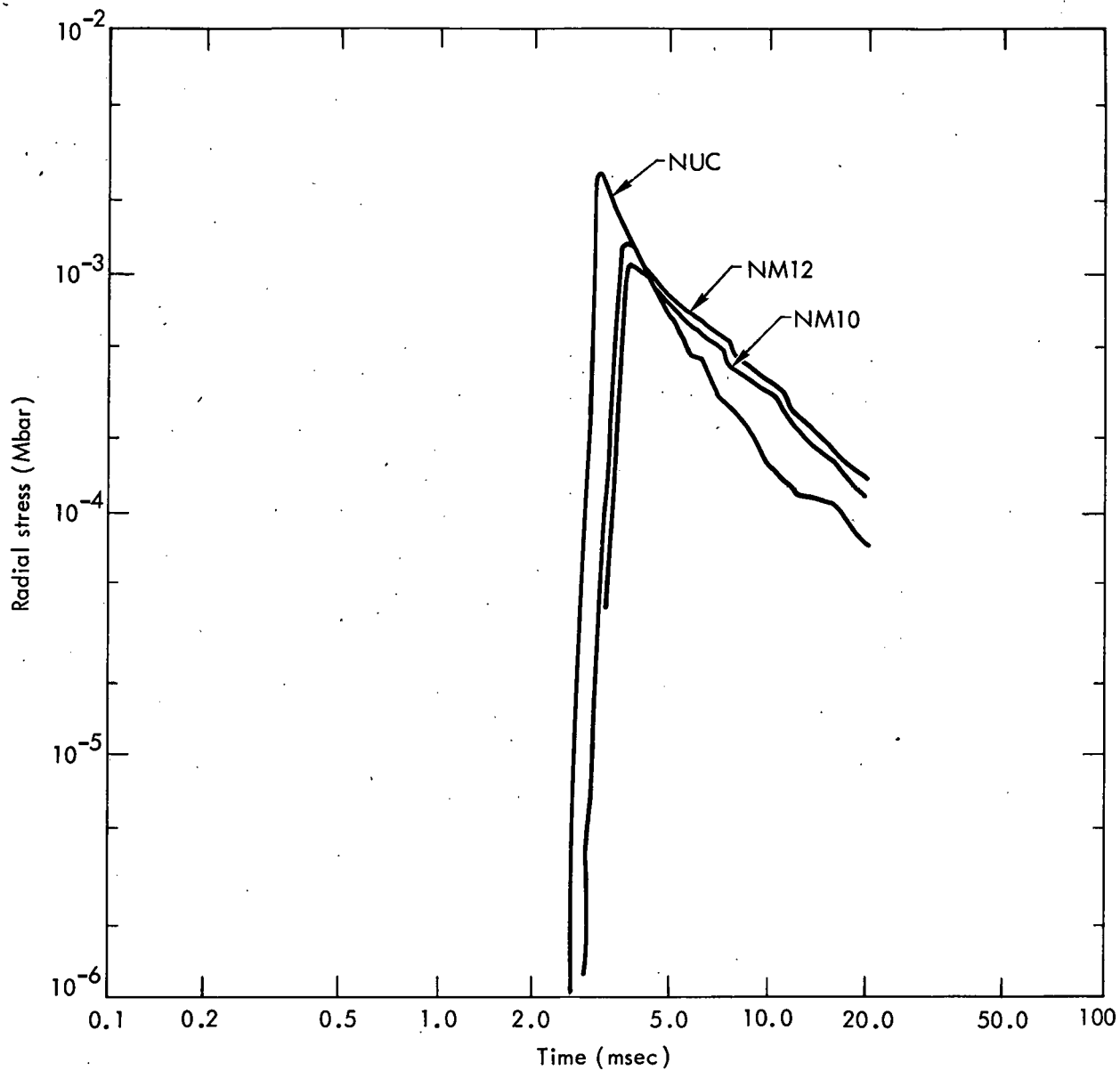

Fig. 4a. Calculated radial stress pulse waveforms as a function of time, Diamond Mine tuff; range = 8 meters from a nuclear detonation, a 12.26-ton energy yield nitromethane detonation, and a 10-ton energy yield nitromethane detonation.

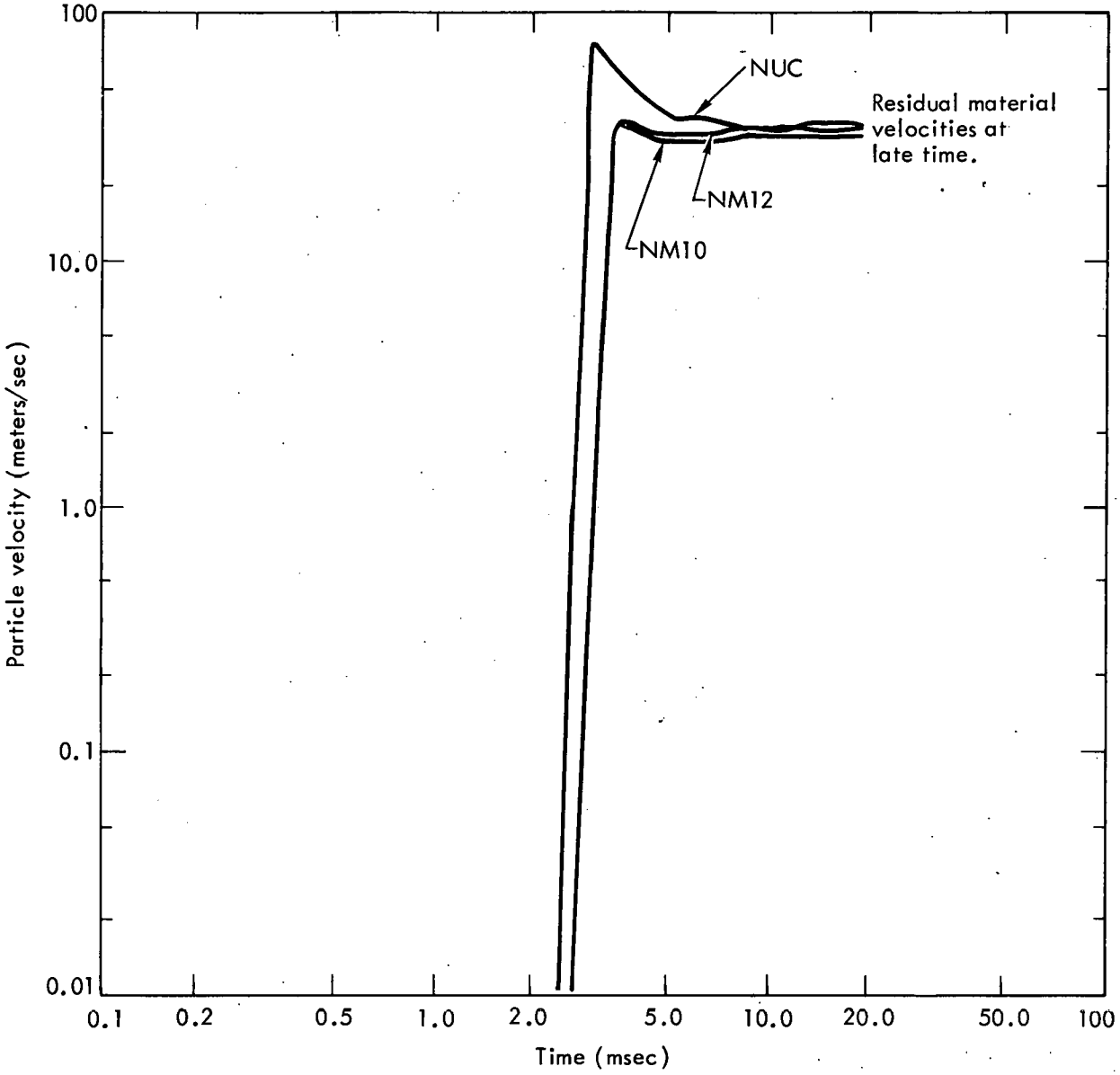

Fig. 4b. Calculated particle velocity waveforms as a function of time; range = 8 meters.

type appears after the peaks have passed. The peaks from the nuclear source are very strongly damped and decline abruptly within a few milliseconds after shock arrival. The radial stresses for the HE calculations, on the other hand, decline more gradually with time and are higher than the corresponding nuclear stresses after 5 msec (Fig. 4a).

A similar trend is reflected in the velocity waveforms, Fig. 4b, which show a sudden decrease in particle velocity after the nuclear shock front passes but very little damping for the HE events (residual velocity behind the front remains almost as high as the peak velocity). Residual velocities for the NUC (20 ton) and NM12 (12,26 ton) calculations are approximately equal at times later than 8.0 msec, while the residual velocities for NM10 fall fractionally lower. The velocity waveforms at ranges between 4 and 20 meters show a similar appearance, with comparable residual velocities for NUC and NM12 at a given range. This range interval is most crucial for material ejection effects from typical cratering detonations.

The velocity waveforms thus suggest that NM12 may be an appropriate similitude analog for the nuclear event in terms of residual velocities and late-time material ejection. Similitude will necessarily be somewhat imperfect in this material due to the considerable differences in peak values. Higher velocities in the nuclear calculation persist for about 2.5 msec after the peak (allowing for the slightly different peak arrival times), then decline to the level of event NM12. In a spatial sense, this corresponds to an interval of roughly 4 meters behind the shock front over which the basic dynamic effects for nuclear and HE events will not be identical. Differences of the early-time waveforms may adversely influence similitude of short time-scale phenomena closely related to the shock peaks; in particular, the near-surface spall velocities for cratering events will be affected. Dynamic interactions that govern the cratering process as a whole encompass time scales longer than 2.5 msec, and are thus best simulated by assuring that kinetic energies and long-term residual velocities are the same.

The major surprise generated by these calculations was the substantial difference between the time-behavior of nuclear and HE waveforms. A clue to the origin of this difference was found by examining the cavity gas behavior for the two types of events. The average cavity pressure is plotted as a function of time in Fig. 4c. Pressure for the nuclear event decreases monotonically, since the shock wave decouples from the high-pressure initial gas source at very early time and the cavity continues to expand thereafter. Pressures for the HE reach a maximum near 0.25 msec (when the explosive burn is complete and the shock wave crosses the HE-rock interface), then decline. These trends are parallel to those observed for Bearpaw shale,[1] but the late-time pressures are noticeably higher in the tuff due to the retarding effect of rock strength on cavity expansion.

Further information is provided by the cavity energy content, shown in Fig. 4d.* For the nuclear calculation, both the cavity energy content (iron gas) and the energy

*Energy content in the cavity gas is almost entirely internal energy; Fig. 4d includes both the internal energy and the small amount of kinetic energy.

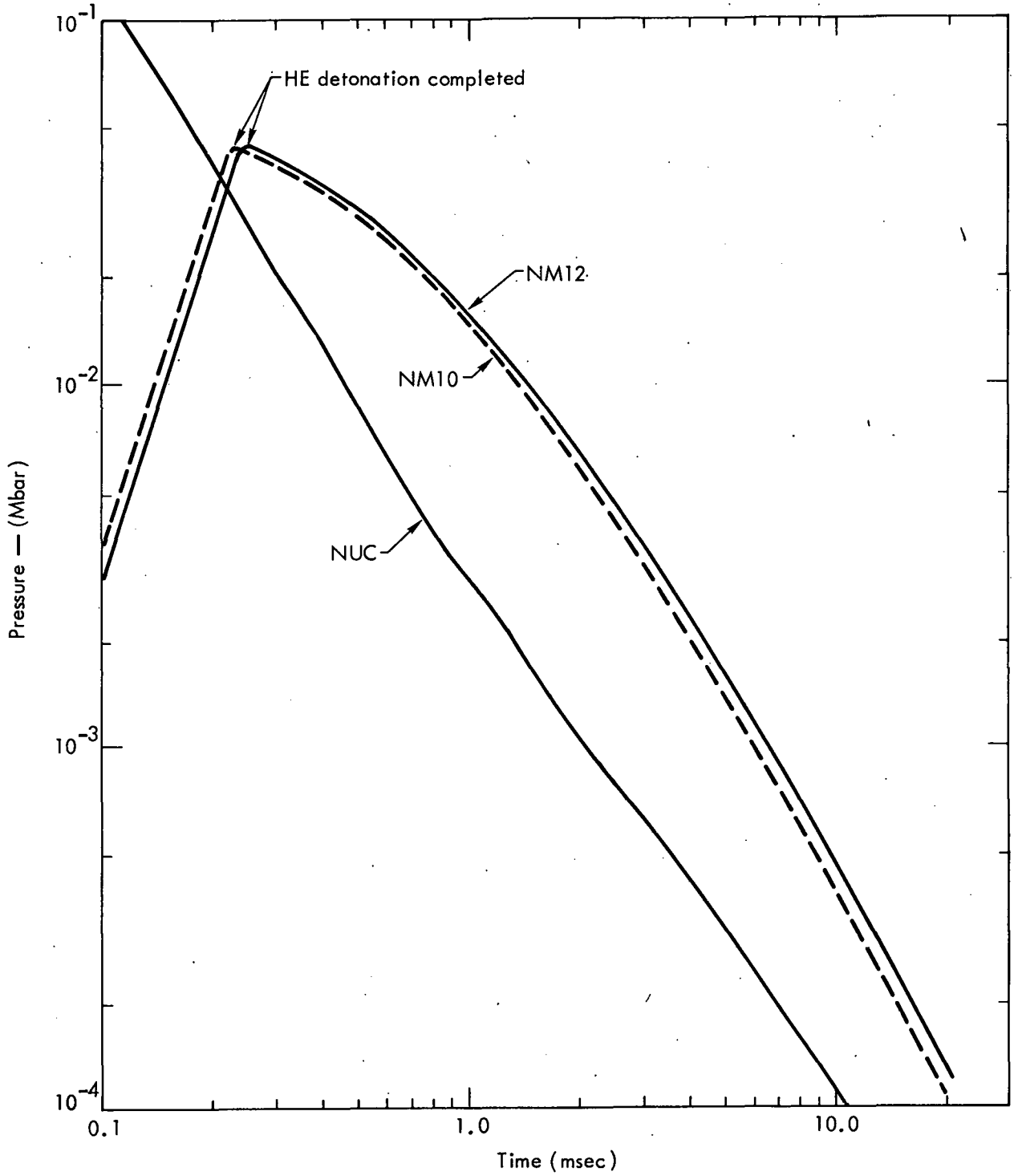

Fig. 4c. Average source pressure in the cavity as a function of time.

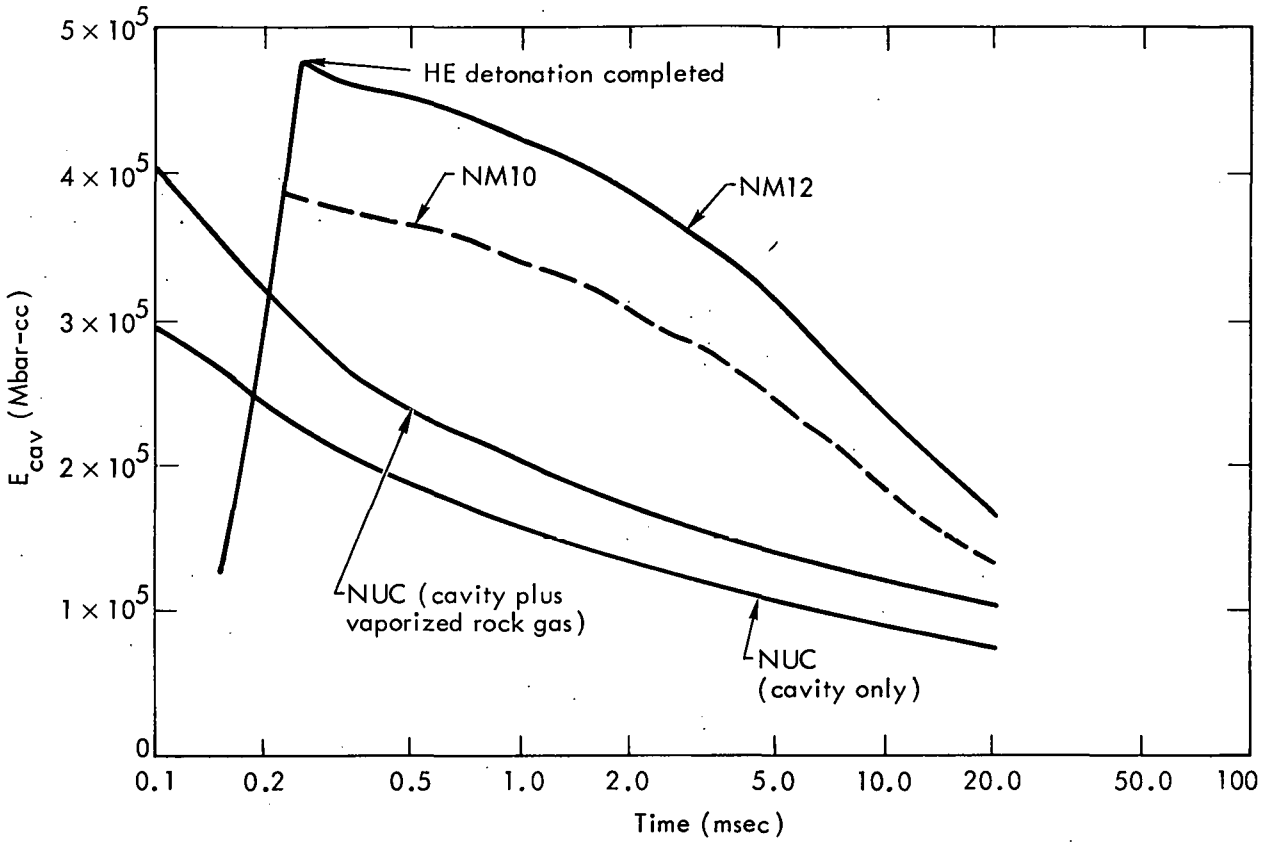

Fig. 4d. Total energy content in the cavity as a function of time.

content in the cavity plus the surrounding mass of vaporized rock gas are plotted, since the rock gas may be considered as part of the late-time source region. The nuclear source energy declines monotonically and is low compared to the HE events, since most of the energy was emitted in the intense initial shock wave. Significantly, the HE cavity energies after 0.25 msec still account for a major portion of the total problem energy, and significant energy transfer from cavity to rock is proceeding at relatively late times. The total energy transferred during any given time interval may be determined from the curves in Fig. 4d. For the NM12 calculation, the cavity-to-rock energy transfer between 1 msec and 20 msec is 2.56×10^5 Mbar-cc (2.56×10^{17} ergs), or 50% of the total problem energy. During the same period, energy transfer for NM10 is 2.10×10^5 Mbar-cc, likewise 50% of the total energy. Late-time energy transfer for the nuclear calculation is only 0.808×10^5 Mbar-cc = 9.7% of the problem energy (cavity only), or 0.978×10^5 Mbar-cc = 11.7% of the problem energy (cavity plus rock gas).

The basic cause of the differing waveforms is now evident. The nuclear source broadcasts almost all of its energy in the strong initial pulse, with very little driving force from the cavity at late times. The HE sources transfer most of the available energy to the rock at much later times between 1 and 20 msec, well behind the initial shock front. The higher HE source pressures also maintain high shear stress levels, matching the strength of the rock. A sustained flow is thus developed behind the shock front, accounting for the high and consistent residual velocities observed in the HE calculations. The sustained energy transfer is quite efficient in converting source energy to kinetic motion, since it occurs under conditions of fairly low pressure (minimal waste heat losses) and low pressure gradient.

The shock waveforms presented above were referred to a standard range of 8 meters. To avoid detailed analysis of the waveforms at all ranges, it is convenient to assign figures of merit to various characteristics of the wave. These may include the peak values, waveform integrals, late-time residual velocities behind the shock front, etc. The peak particle velocities "V_p" at the shock front have been determined for each of the three calculations. These are plotted as a function of initial range in Fig. 5a. The nuclear shock wave attenuates most rapidly with range due to the greater energy losses (less efficient transmission). Nonetheless, peak velocities remain well above both HE events to the outer limit of the calculations. Figure 5b presents the approximate residual velocities at a time several milliseconds after shock passage. These reveal a quite different picture, with the HE event velocities being slightly higher at very close ranges but almost equal to the nuclear event velocities beyond 3 meters.

The total material displacements, which correspond to the integrated velocity over the entire problem history (0 to 20 msec), are given in Fig. 6. Note that the total displacements for the nuclear and HE events are similar, with the NM12 calculation almost perfectly matching NUC. The HE displacements appear to be slightly lower at very long ranges beyond 25 meters; this is a spurious result caused by the earlier arrival of the nuclear shock and the 20 msec termination time imposed on the calculations. The HE signals have just arrived at these long ranges, and the latter part of the waveforms

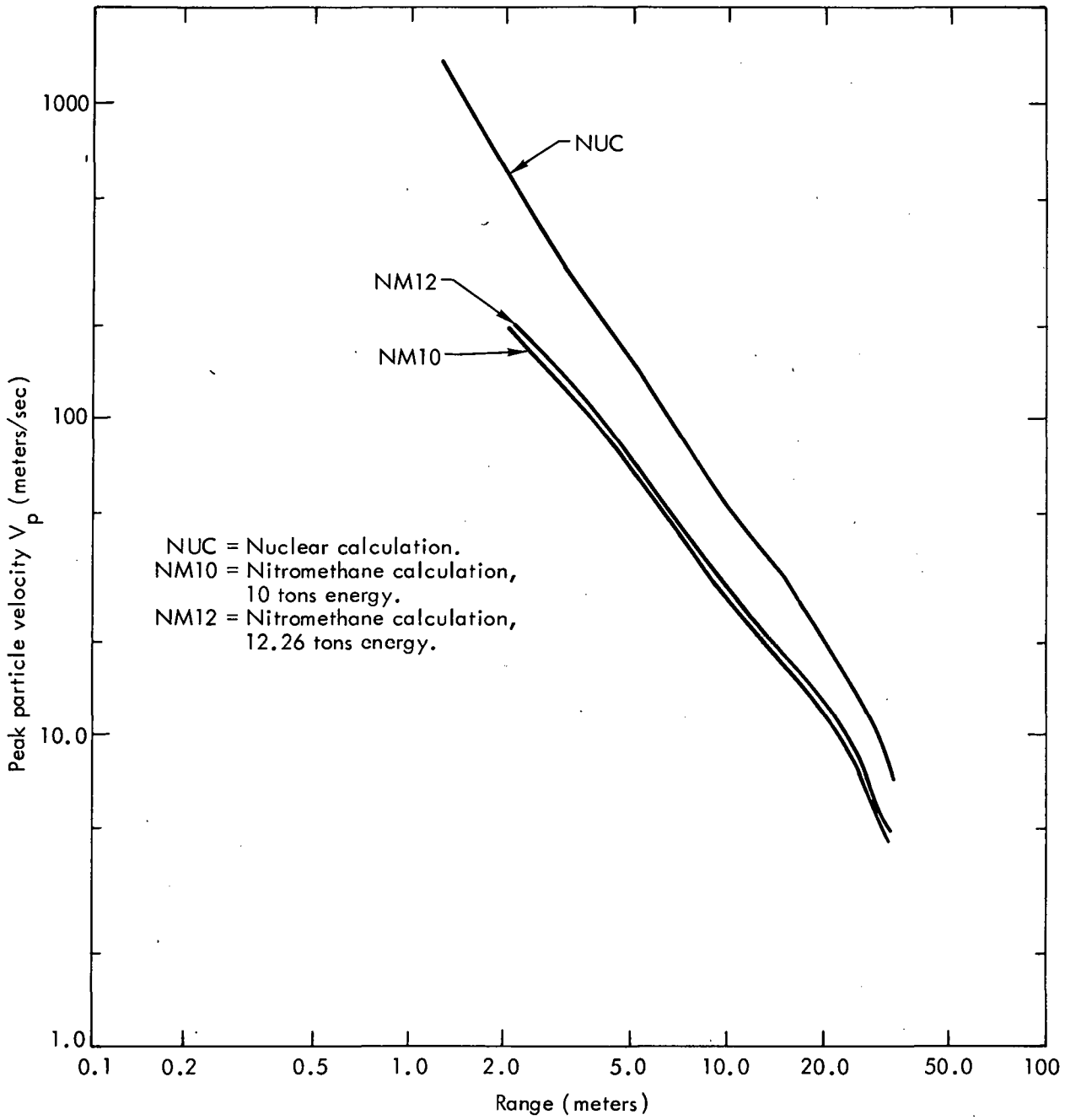

Fig. 5a. Peak particle velocity "V_p" experienced by tuff material as a function of initial range "R."

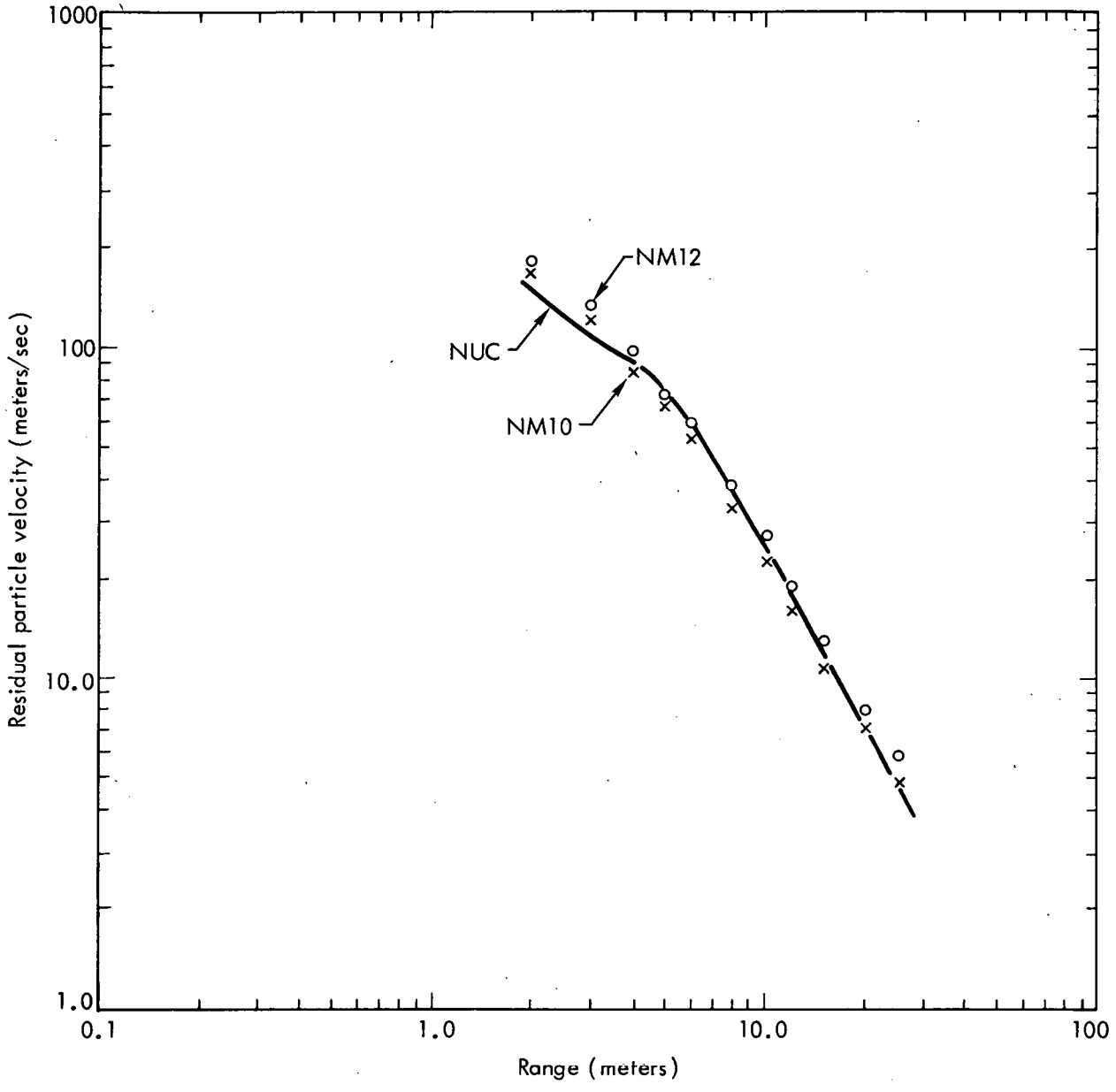

Fig. 5b. Residual particle velocity behind the shock front experienced by tuff material as a function of initial range "R."

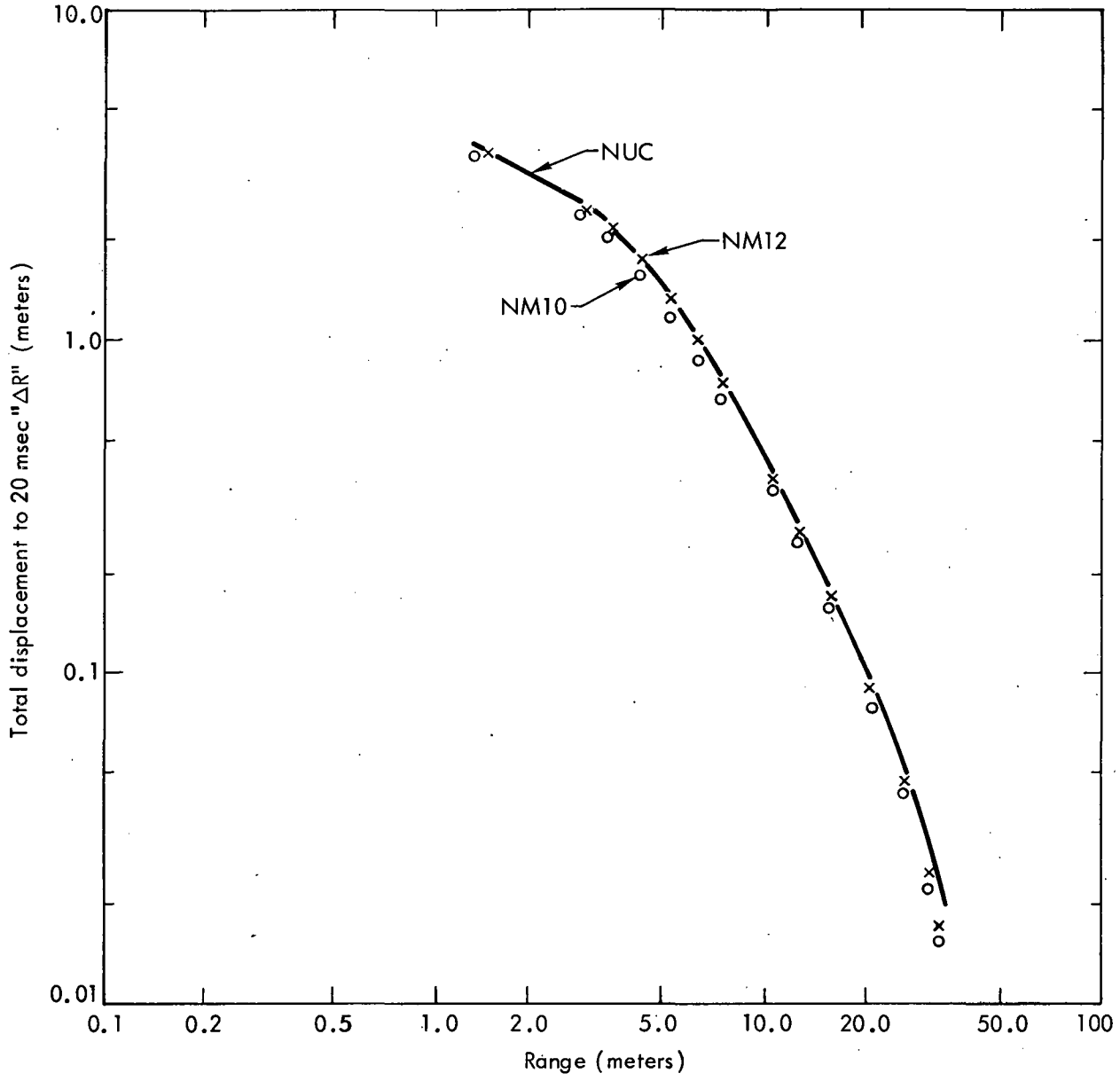

Fig. 6. Total displacement "ΔR" experienced by the tuff material (to a time of 20 msec) as a function of initial range.

is effectively truncated. This small disagreement could be avoided by running the HE calculations about 0.7 msec longer to allow comparable accumulation of shock effects.

Figure 7 gives peak pressures "P" experienced by the rock, and Fig. 8 shows peak volumetric compressions "Mu_{max}" (the peak compression is directly related to peak pressure through the material compressibility curve). Trends are similar to those noted for peak velocity: the "nuclear" values are higher at all ranges but attenuate more rapidly with increasing range.

Stress pulse waveforms have also been integrated to permit a comparison of the long-term stress effects (Fig. 9). It is evident that the integrated values are closely comparable for the nuclear and HE events. The best correspondence is obtained between "NUC" and "NM12."

Material damage or extent of fracturing for a rock medium is related to the stress history experienced at a given location. In a region of pronounced inelastic behavior, the integral of the stress pulse is generally more important than the peak stress in determining the degree of damage. The relationships between actual rock damage and the stresses or failure parameters calculated by computer codes have not been defined. However, the currently used rock mechanics model provides an approximate measure of failure effects. When a portion of the medium undergoes shear failure (crosses the specified shear strength failure surface), the code calculates a total distortional strain composed of an elastic portion and a failure shear strain "ε_f". Studies of a high-strength granite have demonstrated that extent of fracture is closely correlated with the cumulative failure shear strain.[3] It was found that intense fracture corresponds to a cumulative ε_f value of about 0.1, while the limit of detectable fracture occurred at $\varepsilon_f \approx 0.01$.

The calculated ε_f-values for the three tuff calculations are plotted versus range in Fig. 10. The NM12 curve coincides closely with the nuclear calculation, while NM10 lies somewhat lower. This result was expected, since the integrated stress histories for "NM12" and "NUC" were similar (Fig. 9). The range of intense fracture is estimated as 10.5 meters, while the limit of detectable fracture extends to 23 meters (NM12). The nuclear "ε_f" values slightly exceed NM12 at very long ranges, an effect that is partially attributable to the problem termination time. Note that these damage estimates refer to spherically symmetric free-field calculations, and do not include the surface tensile reflection that occurs for a cratering event.

An important test of similitude closely related to long-term material displacement and cratering is the kinetic energy transferred to rock. Figure 11 presents kinetic energy content in tuff as a function of time for the three sample calculations. The approximate time at which the high-explosive burn finishes is indicated by a vertical arrow in the figure. It is evident that most of the energy transfer for high-explosive events occurs after 1 msec, whereas the transfer for the nuclear case is essentially complete at a much earlier time and the total kinetic energy in rock declines gradually thereafter. This behavior is consistent with the cavity energy transfer characteristics

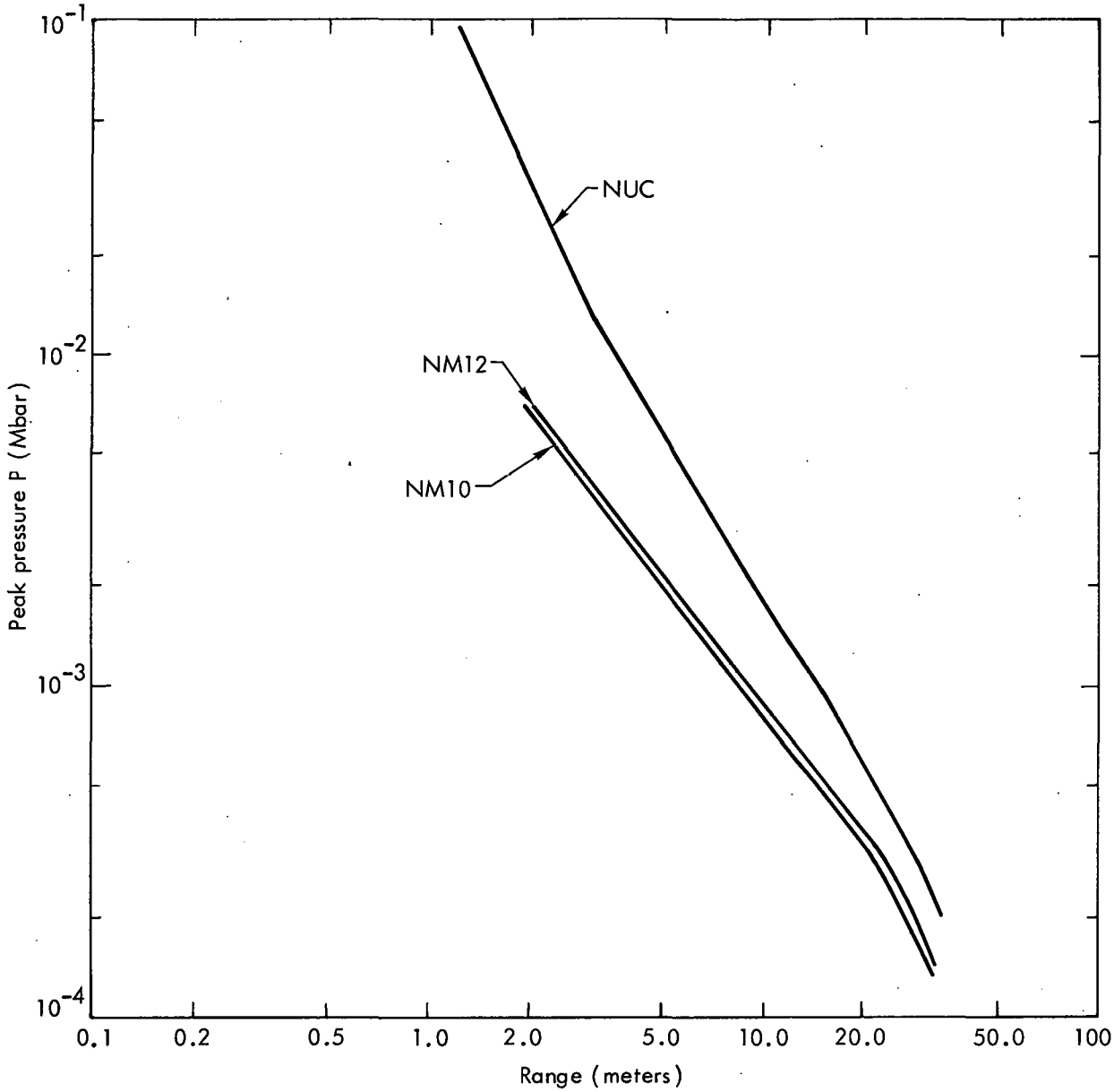

Fig. 7. Peak pressure "P" experienced by the tuff material as a function of initial range.

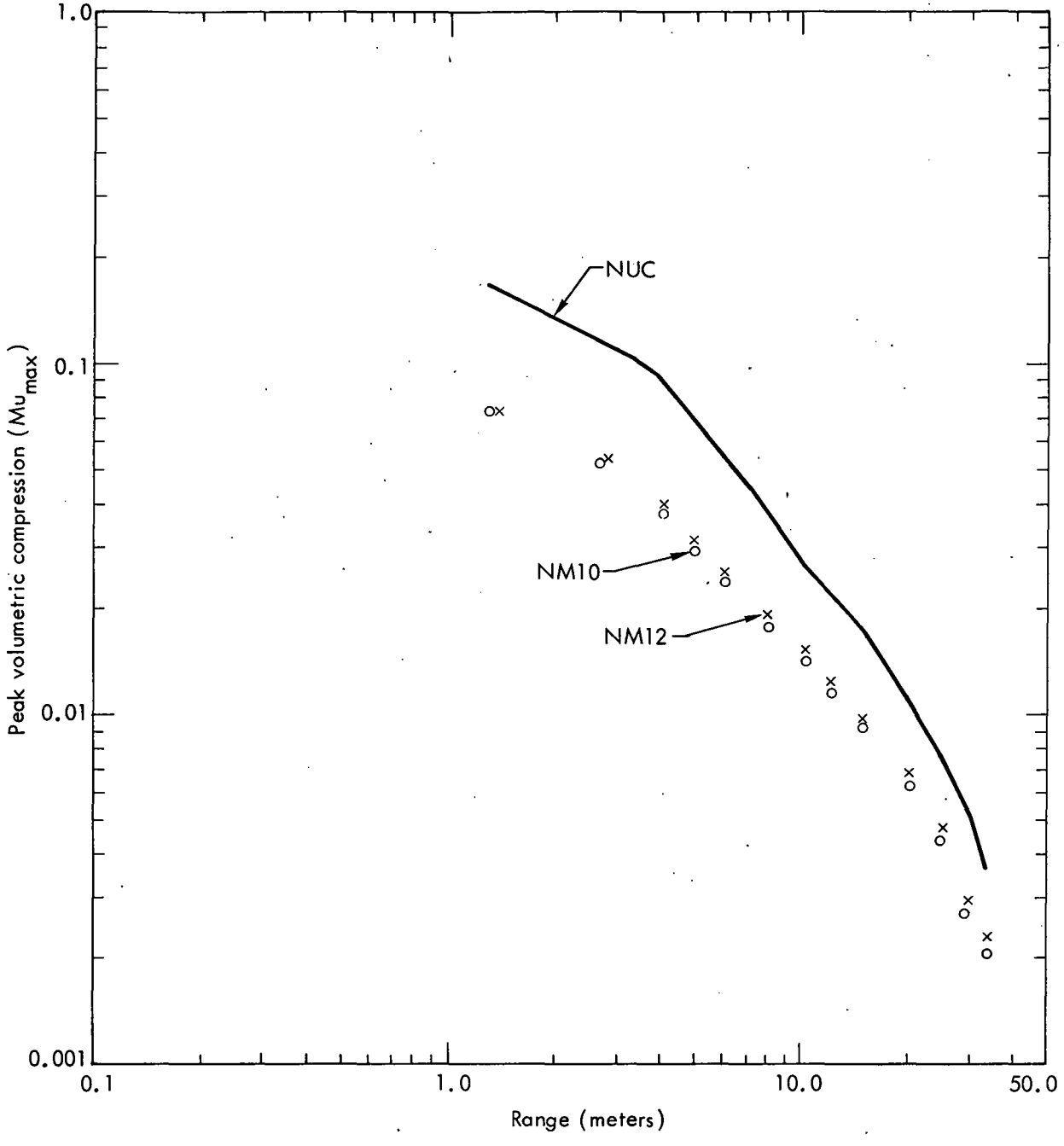

Fig. 8. Peak volumetric compression "Mu_{max}" experienced by the tuff material as a function of initial range.

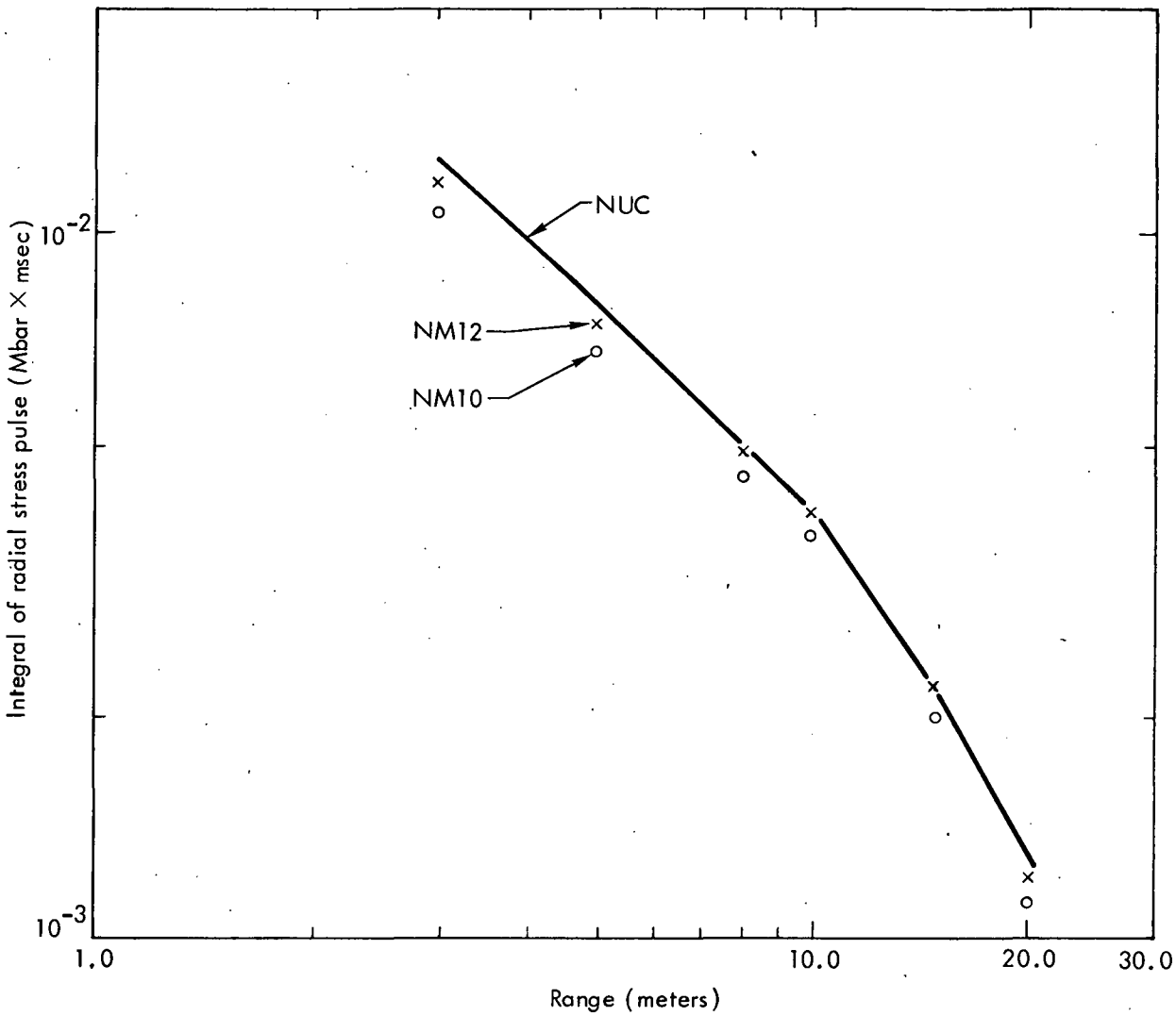

Fig. 9. Approximate early-time integral of radial stress pulse as a function of initial range.

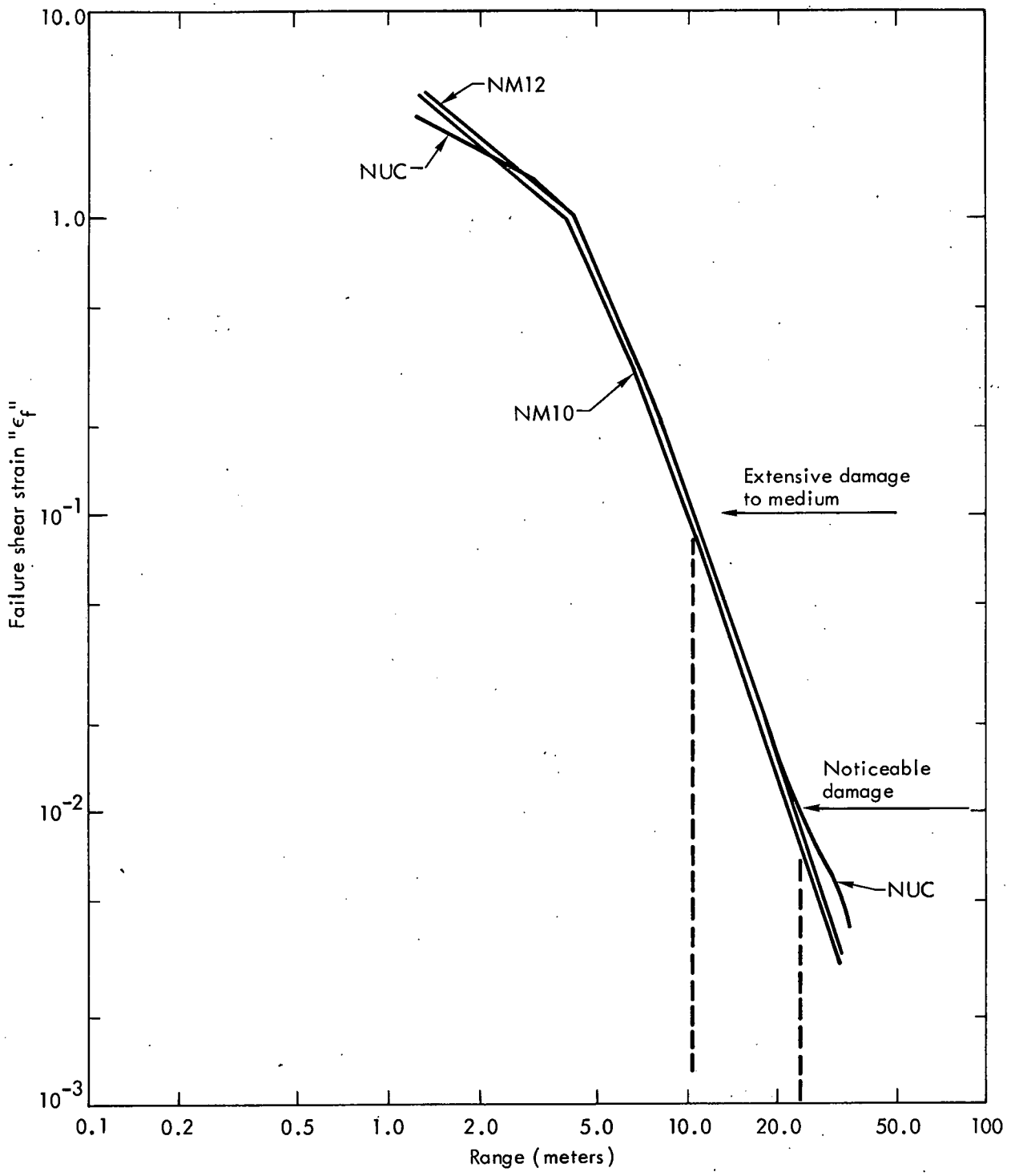

Fig. 10. Failure shear strain "ε_f" experienced by tuff material to 20 msec as a function of initial range.

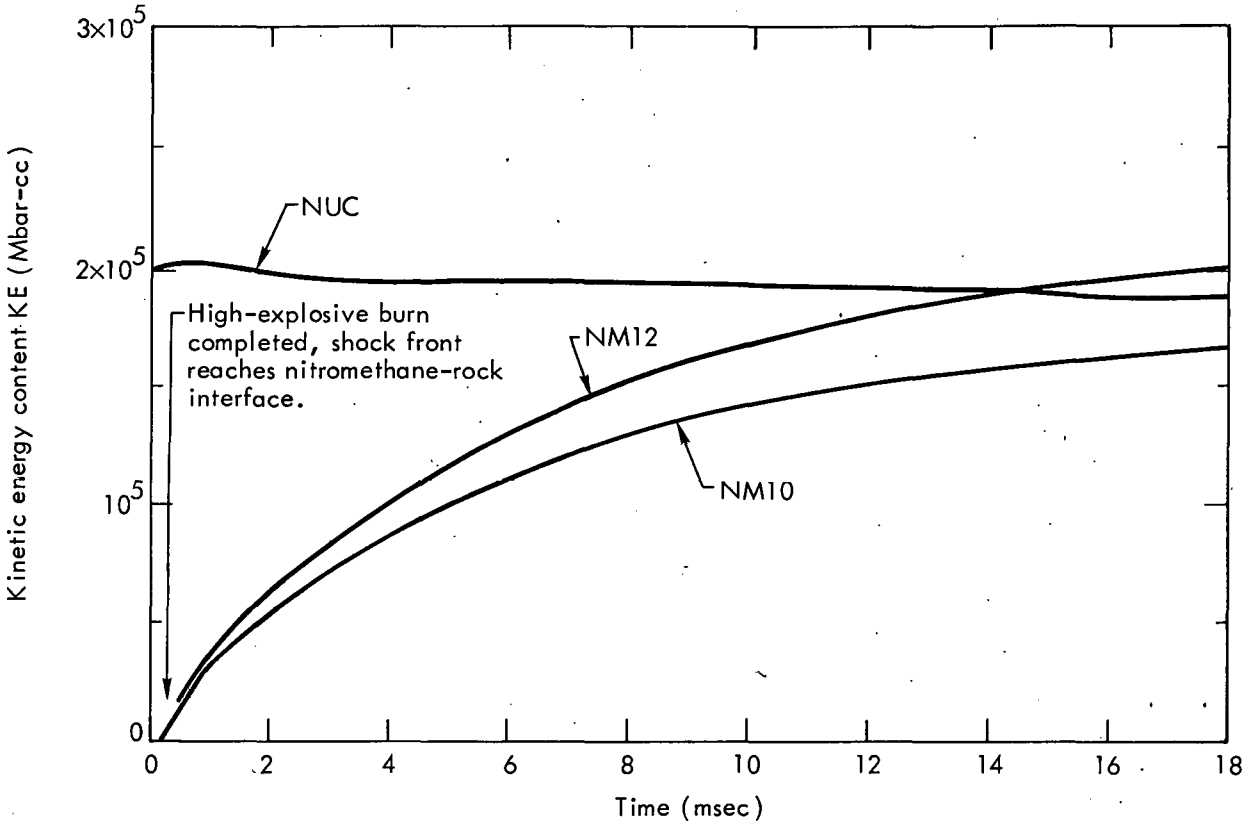

Fig. 11. Kinetic energy content "KE" in the tuff material as a function of time.

and the differences in the velocity waveforms noted earlier. Constrained expansion of the large HE gas cavity causes continuing cavity-to-rock energy transfer at late times and sustained flow of material well behind the shock front (high residual velocities). A similar long-term energy transfer effect was discovered in the one-dimensional high-explosive calculations for Bearpaw shale.[1] However, due to the lower strength and near-fluid behavior of the Bearpaw shale, transfer was complete and the kinetic energy in rock had stabilized by about 4 msec. The tuff calculations reveal continuing and substantial energy increase throughout the 4 to 15 msec time interval. The constraining effect of somewhat higher material strength and the resultant long-term energy transfer associated with cavity expansion account for this prolonged increase. Since energy transfer takes place over a longer period of time, the HE calculations require longer to stabilize and catch up with the nuclear kinetic energy.

In spite of the differences in time-dependent dynamic behavior, the HE and nuclear kinetic energies are seen to compare favorably at times later than 8 to 10 msec. This corresponds approximately with the time at which residual velocities behind the shock become equal in the intermediate range interval (Fig. 4b). The "NM12" kinetic energy in Fig. 11 lies close to the nuclear curve, while "NM10" is somewhat lower than the other two calculations. Thus the 12.26-ton nitromethane event appears well-chosen to simulate dynamic phenomena for the 20-ton nuclear calculation. This result favors an HE/nuclear similitude factor of about 61%, somewhat higher than the value of 50% selected for Bearpaw shale.

Similitude will be valid only for long-term interactions that have effective time scales greater than about 8 to 10 msec. Crater formation by explosive events near optimum burial depth* falls within this category; optimum depth of burial for events of 10 to 20-ton energy yield in wet rock is approximately 12 meters. The stress wave transit time from source to surface is about 5 to 6 msec, and the velocity field within the mound of ejecta material requires approximately two transit times (≈10-12 msec) to stabilize.[1] The total kinetic energy in the ejecta mound and the stabilization time can be accurately determined only by two-dimensional cratering calculations. However, if the kinetic energy at 12 msec is selected as an approximate similitude criterion, we find that 35% of the total HE yield has been converted to rock kinetic energy (about the same as for the Bearpaw shale calculations). The corresponding figure for the nuclear event is 22% (somewhat greater than for the Bearpaw shale calculations). These values produce an HE/nuclear similitude factor of 63%, comparable to the energy difference factor of 61% adopted for the two sample calculations (NM 12.26 ton/NUC 20 ton). Similitude is attainable in this case because material ejection and crater formation depend primarily on the overall kinetic energy coupled to the ejecta mound.

*"Optimum burial depth" is defined as the depth of burial required to maximize the apparent volume of the excavated crater for a given explosive source and medium.

The coupling process for optimum depth detonations occurs over a region that is large relative to the narrow nuclear shock peak. This situation will not apply to shallowly buried shots at depths less than a few meters. For these events, nearness of the free surface invalidates long-term energy coupling estimates made from the one-dimensional calculations. Material ejection will be controlled by high-velocity spall launch over a much smaller near-surface region, comparable in size to the nuclear shock peak. Velocities and kinetic energies will thus be partly dependent on peak values near the shock front. As was shown earlier, the peak velocities are much higher for the nuclear calculation. Correct similitude of the peak values and long-term material motion cannot be attained at the same time for this material.

DISCUSSION

Differences between the tuff and Bearpaw shale calculations[1,2] are directly attributable to the basic material properties. The tuff is much higher in strength and much less fluid in consistency. Relative energy losses to internal heating are less severe for the tuff nuclear calculation. The transient peak from the nuclear source is transmitted efficiently, and peak values at the shock front are quite high. However, the high peak velocities are rapidly damped in this stronger material after the front passes. Peak velocities and stresses at equivalent ranges for the high-explosive calculations are considerably lower, but these small peak values are compensated by the much slower decay and higher residual velocities behind the front.

The dramatic change in behavior between nuclear and HE calculations reflects the importance of late-time cavity expansion, which is the dominant mechanism for transforming HE gas energy to rock motion in this medium. Cavity growth is restrained but not abruptly halted by the moderate strength of the tuff material. Relatively high stress levels are thus maintained near the cavity, and energy transfer to the rock is spread over a long time interval. The long-term expansion induces sustained flow of material behind the shock front, and the relatively low strength assures efficient conversion of the cavity driving force to kinetic energy of the rock. This energy transfer mechanism is so efficient that the late-time residual velocities at ranges beyond 5 meters are almost as high as the peak velocities at the shock front. The long-term residual velocities at ranges near or beyond 5 meters exert a critical influence on the overall material dynamics and crater formation.

No corresponding energy transfer mechanism is effective for the nuclear case, since most of the device energy is emitted with the intense initial shock wave; late-time cavity pressure and cavity energy content are comparatively small, and cavity expansion does not contribute significantly to the rock kinetic energy. Due to the lack of continued strong driving impulse from the cavity, deceleration and strength effects cause residual velocities to drop well below peak values; kinetic energy in the rock does not increase at late times. The differing mechanisms and time-scales of

energy transfer account for the deviations between the nuclear and HE events: calculated peak values and early-time kinetic energies for the nuclear example far exceed the corresponding HE parameters, while the residual velocities and late-time energies for the HE events ultimately approach or surpass the nuclear calculation. The extended duration of the cavity expansion phase means that kinetic energy transfer continues to late time. Rock kinetic energy for the HE similitude event in tuff does not approach the nuclear calculation until about +10 msec.

CONCLUSIONS

Comparative calculations for high-explosive and nuclear events in weak wet tuff have shown that the shock transmission properties differ somewhat from the previously-studied Bearpaw shale material. Nonetheless, final similitude requirements are not grossly dissimilar. It was found that a nuclear detonation provides the same amount of kinetic energy to the tuff environment as a high-explosive event equal to about 60% of the nuclear energy yield. This estimate of the similitude value is smaller than other estimates which range from 75 to 100%.

Comparison of the tuff nuclear calculation and its high-explosive similitude analog reveals that the peak pressures and velocities at the shock front are about a factor of two higher for the nuclear case. Thus, transient phenomena closely related to the shock peak cannot be accurately simulated. Long-term mechanical coupling from the high-explosive gas cavity greatly increases kinetic energy transfer at late times, producing high residual velocities that compensate for the lower peak values. Thus, total kinetic energy transfer, long-lived material motion, and other integrated effects can be properly simulated between the nuclear and HE calculations. These include residual velocities behind the front, total displacements, integrated stresses, and cumulative fracture damage to the rock. Strength effects play a complex but important role in enhancing the long-term coupling efficiency for HE events and in extending the energy transfer process over a longer period of time.

Modeling accuracy for subsidiary effects will be dependent upon the time-scale over which they occur and the relationship to the shock peak. In general, long-term interactions that encompass a time scale greater than a few milliseconds (width of the intense nuclear peak) will be properly simulated. Long-range free-field effects such as distant seismic motion are probably most closely related to the integral of the velocity waveform near the elastic radius; thus, satisfactory modeling should be attained for parameters of this type. Very rapid close-range interactions will be poorly matched, including the near-surface spall velocities in the narrow surface layer above a cratering event. Likewise, the ground-shock-induced airblast wave, which is induced by the early-time surface peak spall velocity and rapidly decouples from the rising mound surface, cannot be accurately modeled. These effects appear to be less well simulated for the tuff medium than for the previous Bearpaw shale calculations, since the transient

peak values were found to differ substantially between the nuclear and HE tuff events. Precise modeling of spall velocities in the narrow surface layer is not essential to cratering similitude, since most of this material is launched with high velocity and rapidly departs the immediate mound vicinity. Correct simulation of crater volume is assured by the successful modeling of total kinetic energy and overall mound velocities.

Results of these tuff calculations are influenced by the unique physical properties of the material, particularly the assumed strength and the nearly saturated compressibility behavior. The strength of the tuff is small but not negligible in relationship to the stresses prevailing at and behind the shock front. It therefore acts to limit shear stresses on loading near the front and to retard, but not completely halt, cavity expansion behind the front. This behavior is crucial to the maintenance of high stresses and sustained flow observed for the HE calculations. Dramatically different results might be expected for a high-strength rock which slows cavity growth at an earlier time. Similarly, the effects of hysteresis (permanent compaction of air voids) have not yet been investigated. Hysteresis is strongly dependent upon the peak pressure achieved, and may be an important phenomenon for porous materials at the intermediate pressure levels be an important phenomenon for porous materials at the intermediate pressure levels reached during crater formation. Note that peak pressure was not accurately modeled between HE and nuclear events in this study (non-hysteretic tuff material).

The similitude results presented in this report are based on one-dimensional spherically symmetric calculations for a saturated tuff. Another recent study[10] was concerned with high-explosive and nuclear effects in very weak soil media. Both one-dimensional and two-dimensional calculations were performed for materials characteristic of the ESSEX Program experimental sites at Ft. Polk, Louisiana. Saturated soils and unsaturated porous media were included in the investigation. Material strengths were much lower than the tuff used in the current study. More complicated emplacement geometries were considered, including vertically layered sites, shallow burial depths, variations in charge shape, and unstemmed (open) emplacement holes. The high-explosive/nuclear similitude factors for energy coupling (one-dimensional calculations) and cratering effectiveness (two-dimensional calculations) ranged from 40% to 58%, depending on the material properties and emplacement geometry.[10,11] Results of the two-dimensional ESSEX calculations also demonstrated that similitude for cratering events can sometimes be improved by a judicious choice of the HE charge shape and emplacement configuration. Cratering calculations similar to the ESSEX work would provide more detailed information about similitude and HE/nuclear effects in tuff media. Such detailed calculations are most appropriate after an emplacement design has been selected and the site material has been accurately characterized.

REFERENCES

1. D. Burton, C. Snell, and J. B. Bryan, Computer Design of High-Explosive Experiments to Simulate Subsurface Nuclear Detonations, Lawrence Livermore Laboratory, Rept. UCRL-75190 Rev.1 (1974).
2. J. B. Bryan, D. E. Burton, and M. D. Denny, Numerical Studies of Cratering in Bearpaw Shale: Two-Dimensional Results, Lawrence Livermore Laboratory, Rept. UCRL-51659 (1974).
3. J. F. Schatz, SOC73, a One-Dimensional Wave Propagation Code for Rock Media, Lawrence Livermore Laboratory, Rept. UCRL-51689 (1974).
4. E. Lee, H. Hornig, and J. Kury, Adiabatic Expansion of High-Explosive Detonation Products, Lawrence Livermore Laboratory, Rept. UCRL-50422 (1968)
5. F. Helm, R. Boat, M. Finger, and D. Wooster, ESSEX-DIAMOND ORE RESEARCH PROGRAM: The Development and Manufacture of a Gelled Nitromethane Explosive for Project ESSEX, Lawrence Livermore Laboratory, Rept. UCRL-51536 (1974).
6. T. R. Butkovich, The Gas Equation of State of Natural Materials, Lawrence Livermore Laboratory, Rept. UCRL-14729 (1967).
7. T. R. Butkovich, A Technique for Generating Pressure-Volume Relationships and Failure Envelopes for Rocks, Lawrence Livermore Laboratory, Rept. UCRL-51441 (1973).
8. H. C. Heard, R. N. Schock, and D. R. Stephens, High-Pressure Mechanical Properties of Tuff from the Diamond Mine Site, Lawrence Livermore Laboratory, Rept. UCRL-51099 (1971).
9. B. K. Crowley, D. E. Burton, and J. B. Bryan, Bearpaw Shale: Material Properties Derived from Experiment and One-Dimensional Studies, Lawrence Livermore Laboratory, Rept. UCID-15915 (1971).
10. J. M. Thomsen and H. D. Glenn, Numerical Cratering Studies for Project ESSEX-I, Phase I, the 12 MS Experiment, Lawrence Livermore Laboratory, Rept. UCRL-51771 (1975) (title U, report Confidential).
11. J. M. Thomsen, Lawrence Livermore Laboratory, private communication (1975).

JDT/1c

Printed in the United States of America
Available from
National Technical Information Service
U. S. Department of Commerce
5285 Port Royal Road
Springfield, Virginia 22151
Price: Printed Copy $___*; Microfiche $2.25

*Pages	NTIS Selling Price
1-50	$4.00
51-150	$5.45
151-325	$7.60
326-500	$10.60
501-1000	$13.60